

Stereodynamical Control of Cold Collisions of Polyatomic Molecules with Atoms

Dongzheng Yang, Daiqian Xie,* and Hua Guo*



Cite This: *J. Phys. Chem. Lett.* 2022, 13, 1777–1784



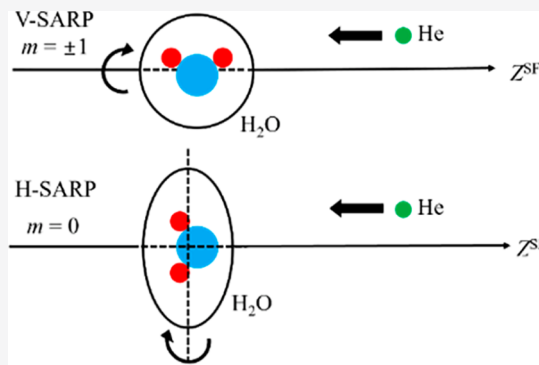
Read Online

ACCESS |

Metrics & More

Article Recommendations

ABSTRACT: Scattering between atomic and/or molecular species can be controlled by manipulating the orientation or alignment of the collision partners. Such stereodynamics is particularly pronounced at cold (~ 1 K) collision temperatures because of the presence of resonances. Comparing to the extensively studied atomic and diatomic species, polyatomic molecules with strong steric anisotropy could provide a more sophisticated platform for studying such stereodynamics. Here, we provide the quantum mechanical framework for understanding state-to-state stereodynamics in rotationally inelastic scattering of polyatomic molecules with atoms and apply it to cold collision of oriented H_2O with He on a highly accurate potential energy surface. It is shown that strong stereodynamical control can be achieved near 1 K via shape resonances. Furthermore, quantum interference in scattering of a coherently prepared initial state of the H_2O species is explored, which is shown to be significant.



One of the holy grails for molecular and chemical physicists is to accurately control the scattering dynamics at the quantum state level. This is often achieved at ultracold or cold conditions where only one or few partial waves are relevant.^{1,2} One such approach is to create ultracold molecules in a single quantum state, e.g., KRb, directly from ultracold atoms (K and Rb), using STIRAP (stimulated Raman adiabatic passage).^{3,4} These ultracold KRb molecules are then allowed to interact near ~ 250 nK, revealing reaction dynamics with both quantum state resolution and partial wave selection.^{5,6} An alternative approach is to lower the collision temperature of the colliding species to a few kelvin. This can be achieved by either decelerating molecules with external fields,^{7–9} or controlling the relative collision velocity by copropagating the collision partners.^{10–13} The latter approach also allows internal excitation of the transitionally cold molecules, creating conditions far from thermal equilibrium.

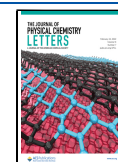
A complete description of collision dynamics requires the precise control of not only the translational energy, partial wave/impact parameter, and internal quantum state(s) but also the collision geometry, namely the relative orientation/alignment of the collision partners. This so-called stereodynamics stems from the anisotropy of the interaction potential energy surface (PES).^{14,15} Cold conditions necessarily restrict the scattering to the lowest few (sometimes one) partial waves, which accentuate stereodynamics. A recent ultracold experiment with oriented KRb molecules, for example, revealed strong orientation dependence of bimolecular reactivity controlled by long-range dipole–dipole

interaction.¹⁶ Hence, cold collision offers a unique way to probe weakly interacting regions of the PES, particularly the long-range interaction,¹⁷ as the collision partners often form metastable complexes referred to as resonances.¹⁸ In a series of landmark experiments, Mukherjee, Zare, and their co-workers investigated cold collisions between copropagating species, including He, H_2 , HD, and D_2 , and found strong stereodynamics.^{10,11,19–22} In these experiments, one or both collision partners were prepared in a single quantum state via Stark-induced adiabatic Raman passage (SARP) with orientation (or alignment) at particular angles to the collisional axis.^{23,24} Strong differences between the different orientation/alignment scenarios were detected in the differential cross section, which were attributed to threshold shape resonances for partial waves with low orbital angular momentum quantum numbers (L). Note that these resonances are not detectable in ultracold collisions as they are mostly present in the cold (~ 1 K) regime, controlled by the weak intermolecular interaction between the collision partners. Theoretical investigations on the benchmark rotationally inelastic scattering between H_2 and oriented HD molecules confirmed this interpretation,^{25,26} and this suggested

Received: January 20, 2022

Accepted: February 14, 2022

Published: February 15, 2022



further ways to control the stereodynamics.²⁷ Extensions to other diatom–diatom systems have also been proposed.^{28,29} However, the reproduction of SARP results for the scattering of aligned HD by He was not entirely successful,³⁰ underscoring the complexity in precise theory–experiment comparison.

So far, such stereodynamical studies have been restricted to diatomic molecules. Polyatomic molecules, in particular asymmetric rotors, are expected to present more pronounced and richer stereodynamical effects, because the PES anisotropy is potentially much stronger and more complex than that of diatoms. Understanding of the stereodynamics involving polyatomic molecules is thus of great importance. In this Letter, we provide the necessary theoretical framework for analyzing stereodynamics in collision of an oriented polyatomic asymmetric top with an atom and report its application to cold collision of oriented water molecules (H₂O) with He atoms. This system is of great importance in understanding the rotational distribution of interstellar water,³¹ and the scattering dynamics has been extensively investigated.^{32–38} Quantum scattering calculations for rotationally inelastic processes in this system reported here reveal strong stereodynamics, particularly near low-lying shape resonances. This new insight helps to advance our understanding of quantum nature of scattering processes.

In this work, we restrict our discussion to rotationally inelastic scattering between a rigid polyatomic asymmetric top with a closed shell atom, as the extension to symmetric or spherical rotor is trivial. Although the oriented molecule in SARP experiments is also vibrationally excited, the vibrational modes have often too high frequencies to strongly couple with the translational and rotational degrees of freedom. Hence, these vibrational degrees of freedom in the polyatomic molecule are assumed to be adiabatically separable. Although their inclusion presents no fundamental problem for atom–triatomic cases as we illustrated recently,³⁹ the lack of full-dimensional PESs presents practical difficulties.

A molecular internal state (MIS) for an asymmetric rotor, which labels the rotational state of the molecule before (without prime) or after the scattering (with prime), can be denoted by $\alpha \equiv (j_{k_a, k_c} P_{\text{ex}})$, with the rotational quantum number j and its projections k_a and k_c onto its a and c principal rotation axes, respectively. Here, only j is a good quantum number. For A₂B type molecules, $P_{\text{ex}} = +1$ labels an MIS with the symmetric nuclear-exchange parity (*para*-H₂O) and $P_{\text{ex}} = -1$ for the antisymmetric one (*ortho*-H₂O). Atomic units are used throughout this Letter unless specifically mentioned.

The scattering calculations were carried out based on our recently published full-dimensional time-independent close-coupling algorithm,³⁹ which yields the state-to-state scattering matrix (S -matrix) as a function of collision energy for atom–triatom collisions. The time-independent approach is ideally suitable for cold collisions where the de Broglie wavelength is long. The calculations were performed on an interaction PES developed by Hou et al.,⁴⁰ which is based on high-level ab initio data and has the correct description of the long-range electrostatic and dispersion interaction. Importantly, the PES used in this work was fit to ab initio data after averaging over the ground vibrational state of H₂O. The quantum scattering calculations were restricted to three active intermolecular coordinates as the PES treats H₂O as a rigid rotor, and such reduced dimensionality treatment is similar to those used by

others.^{41,42} The rotational energy levels used in this work can be found in our previous publication.³⁹

For analyzing the stereodynamics, it is convenient to express the S -matrix in the space-fixed (SF) representation with each collision channel labeled by (αL) where L is the orbital angular momentum quantum number. The scattering amplitude is calculated in terms of the T -matrix elements as^{41,42}

$$q_{\alpha' m' \leftarrow \alpha m}(\theta, E_c) = \frac{1}{2k_\alpha} \sum_j (2J+1) \sum_{L'L} i^{L-L'+1} T_{\alpha'L',\alpha L}^{J_e}(E_c) d_{m,m}^J(\theta) \times \langle j' m' J(-m') | L' 0 \rangle \times \langle j m J(-m) | L 0 \rangle. \quad (1)$$

Here, m is the projection of j onto the SF z axis, which specifies the orientation of the molecule. It is also the projection of J onto the same axis. The orbital angular momentum is defined as $\vec{L} = \vec{J} - \vec{j}$ ($L' = J' - j'$), k_α is the channel wave vector, $d_{m,m}^J(\theta)$ is the Wigner's reduced rotational matrix with scattering angle θ , E_c is the collision energy, and $\langle \dots \rangle$ is a Clebsch–Gordan coefficient. The T -matrix is conventionally calculated from the S -matrix by $T = I - S$, where I is the identity matrix. We note that the summation over all allowed L implicitly includes the summation over both odd and even space inversion parities $\varepsilon = \pm 1$.

In a typical SARP experiment,²³ the molecule is prepared in the same initial MIS, but with its principal axis at an angle relative to the collision axis. These spatially distinct configurations are described in general by the superposition of substates with different m quantum numbers:

$$|\alpha\rangle^{\text{ori},(\beta)} = \sum_m b_m^{\text{ori}}(\beta) |\alpha, m\rangle \quad (2)$$

where $b_m^{\text{ori}}(\beta) = d_{m=0,m}^j(\beta)$. β is the angle between the linear polarization of the SARP laser and the beam velocity. The projection of j onto the laser polarization axis (\hat{m}) is fixed as 0. Therefore, the coefficients in eq 2 are determined by the experiment: $\beta = 0$ is referred to as H-SARP, while $\beta = \pi/2$ is referred to as V-SARP. Note that β can in general have other values, serving as an experimentally tunable parameter.^{20,27}

Similar to atomic scattering of oriented/aligned diatoms,^{43,44} the differential cross section (DCS) for the state-to-state rovibrational inelastic scattering of oriented polyatomic molecules by atoms is

$$\frac{d\sigma_{\alpha' \leftarrow \alpha}^{\text{ori},(\beta)}(\theta, E_c)}{d\Omega} = \sum_{m'} \left| \sum_m b_m(\beta) q_{\alpha' m' \leftarrow \alpha m}(\theta, E_c) \right|^2 \quad (3)$$

where $d\Omega \equiv \sin \theta d\theta d\phi$ is the infinitesimal solid angle. We note that an initial aligned state may not be a “pure” m -labeled substate. This characteristic allows quantum interference between different initial m -labeled substates, which is manifested by the coherent sum of scattering amplitudes over m within the square in eq 3. However, the summation over final m' substates is carried out incoherently, since the final substates are not distinguished by their spatial orientation/alignment. The corresponding integral cross section (ICS) is calculated by integrating over the scattering angle:

$$\sigma_{\alpha' \leftarrow \alpha}(E_c) = 2\pi \int_0^\pi \frac{d\sigma_{\alpha' \leftarrow \alpha}(\theta, E_c)}{d\Omega} \sin \theta d\theta \quad (4)$$

The scattering of oriented molecules can be contrasted with the randomly oriented case, where all m -substates are incoherently distributed with the same weight $\sqrt{1/(2j+1)}$. The corresponding DCS can thus be calculated by

$$\frac{d\sigma_{\alpha' \leftarrow \alpha}^{\text{unori}}(\theta, E_c)}{d\Omega} = \sum_{m'm} \left| \sqrt{\frac{1}{2j+1}} q_{\alpha' m' \leftarrow \alpha m}(\theta, E_c) \right|^2 \quad (5)$$

where the summation is done outside the square. The corresponding ICS assumes the more familiar form:

$$\sigma_{\alpha' \leftarrow \alpha}^{\text{unori}}(E_c) = \frac{\pi}{(2j+1)k_\alpha^2} \sum_J (2J+1) \sum_{L'L} |T_{\alpha'L',\alpha L}^J(E_c)|^2 \quad (6)$$

We first focus on the $1_{0,1^-} \leftarrow 1_{1,0^-}$ transition for *ortho*-H₂O. Figure 1a shows the partial wave (L) resolved ICSs (summed

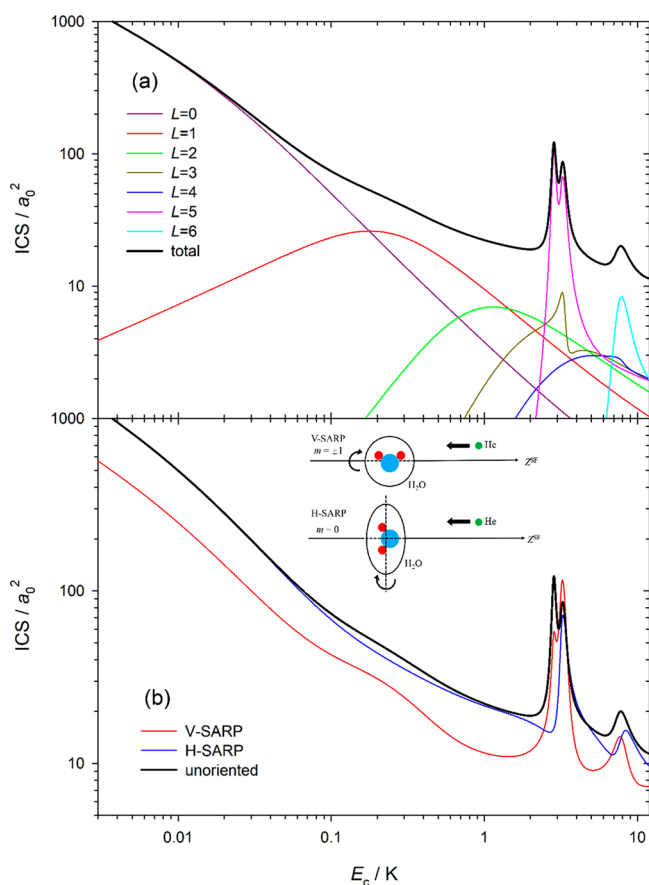


Figure 1. Integral cross sections of the $1_{0,1^-} \leftarrow 1_{1,0^-}$ transition for *ortho*-H₂O + He collision. (a) Partial-wave resolved ICSs. (b) ICSs for different initially oriented H₂O.

over all relevant J s) as a function of the collision energy for unoriented H₂O scattering with He. It is clear that the scattering is dominated by the Wigner threshold law below the collision energy of 0.1 K, where the ICS decreases monotonously and only s -wave contributes to the scattering. The total ICS also shows three resonant peaks in the concerned range of collision energy. The sharp peaks at $E_c = 2.85$ and 7.86 K can be attributed exclusively to $L = 5$ and 6 partial waves, respectively. On the other hand, the resonance at $E_c = 3.24$ K has contributions from both $L = 3$ and 5 partial waves.

For the initial MIS $1_{1,0^-}$, a V-SARP state can be explicitly expressed as,

$$|1_{1,0^-}\rangle^{\text{V-SARP}} = \frac{1}{\sqrt{2}} (|m = +1\rangle - |m = -1\rangle) \quad (7)$$

while the H-SARP one is a pure substate with $m = 0$,

$$|1_{1,0^-}\rangle^{\text{H-SARP}} = |m = 0\rangle \quad (8)$$

Figure 1b compares the ICSs for oriented and unoriented cases. It is clear from the figure that there are significant differences between the two SARP cases. As shown by the inset of Figure 1b, the initial MIS $1_{1,0^-}$ corresponds to the out-of-plane rotation of the water molecule in the classical picture. Therefore, V-SARP or H-SARP leads to a side-on or a head-on collision. In other words, the stereodynamics discussed below is rooted in different orientations of collision partners controlled by the anisotropy of the interaction PES.

The upper panels of Figure 2 show the DCSs as a function of the collision energy and the resonances are also clearly

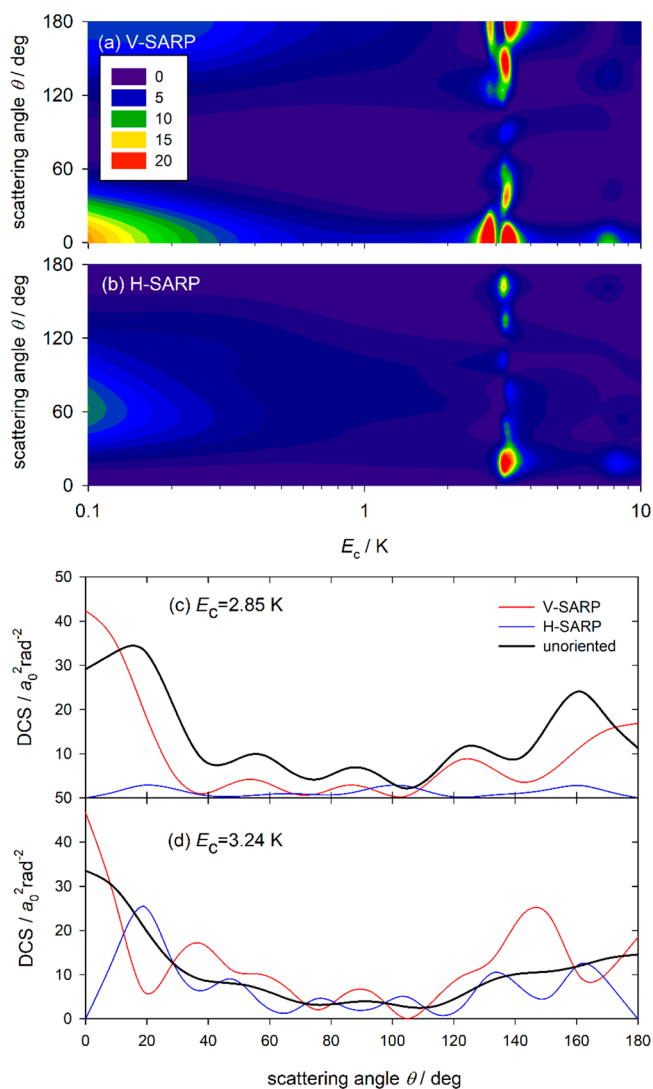


Figure 2. Differential cross sections of the $1_{0,1^-} \leftarrow 1_{1,0^-}$ transition for *ortho*-H₂O + He collision as a function of collision energy and scattering angle for V-SARP (panel a) and H-SARP (panel b), and that at two shape resonant energies of 2.85 (panel c) and 3.24 K (panel d).

visible. The DCS at the two dominant resonance energies are displayed respectively in the lower panels of Figure 2. At $E_c = 2.85$ K, the H-SARP DCS is severely suppressed at all scattering angles, while that of V-SARP case shows strong scattering in both the forward and backward directions. Such differences in DCSs and ICSs are sufficiently significant for experimental verification. At $E_c = 3.24$ K, the difference between the H-SARP and V-SARP is significant, but less pronounced than that at $E_c = 2.85$ K.

In order to gain insight into the nature of the resonances shown in Figure 1a, we calculated the effective potential energy corresponding to different incoming partial waves L as a function of intermolecular distance R

$$V_{\alpha L}^{\text{eff}}(R) = \frac{L(L+1)}{2\mu R^2} + \langle \alpha L | \Delta V | \alpha L \rangle \quad (9)$$

where the first and second terms are, respectively, the centrifugal potential and the diagonal element of interaction potential matrix of the corresponding channel. Figure 3

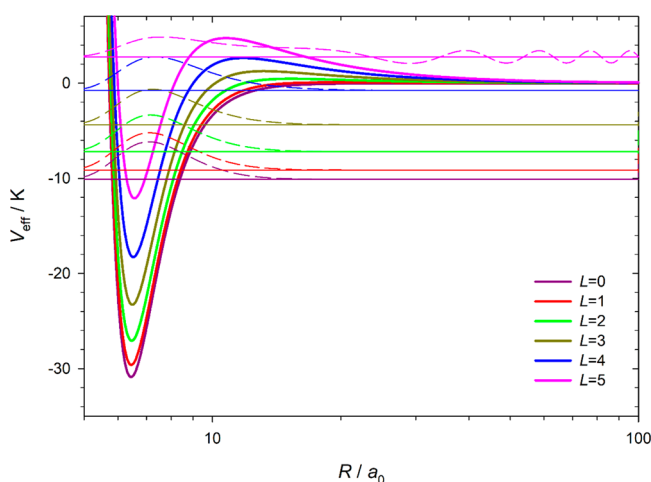


Figure 3. One-dimensional effective potentials and corresponding wave functions of the $\text{H}_2\text{O}-\text{He}$ system as a function of intermolecular distance R .

displays the potential curves for different partial waves, in which the minimum corresponds to the $\text{H}_2\text{O}-\text{He}$ van der Waals complex. In the same figure, wave functions of the bound and quasi-bound states supported by these effective one-dimensional (1D) potentials are also plotted. It is clearly seen that for $L = 0 \sim 4$ only one bound state can be supported by such a shallow van der Waals well. With the increase of L , the eigenenergy of this bound state gradually shifts from -10.10 ($L = 0$) to -0.77 K ($L = 4$). At $L = 5$, the bound state turns into a quasi-bound state with eigenenergy of 2.76 K, which corresponds the shape resonance at $E_c = 2.85$ K for $L = 5$.

The resonance peak at $E_c = 3.24$ K cannot be simply explained by a quasi-bound state on an adiabatic potential, as it has contributions from two L partial waves. To gain insights into its origin, we plot in Figure 4 the trajectory of the S -matrix elements for channels related to the initial MIS, as the collision energy varies from 3.06 to 3.44 K at an interval of 0.014 K, with an arrow pointing to the direction for increasing energy. In the complex plane, a circular trajectory corresponds to an isolated resonance with a long lifetime due to a characteristic phase shift.^{45,46} It is clear that parts a, b, e, and f of Figure 4

show examples of nonresonant scattering, in which the trajectories vary monotonically. On the other hand, trajectories with (half of) a resonant circle can be seen in parts c and d of Figure 4, where both cases are correspondence to ($J = 4, L' = 4$). (Note that the twin resonant peaks at $E_c = 2.85$ and 3.24 K are so close, we can only present S -matrix elements in a very small range of energy, which is responsible for the semicircles.) This observation suggests that the contributions from the $L = 3$ and 5 partial waves to the $E_c = 3.34$ K resonance peak originate from the same outgoing channel $L' = 4$.

The average lifetime of a resonance at a given energy can be characterized by the trace of Smith's lifetime matrix (Q -matrix).⁴⁵ The traces for some selected total angular momenta are shown in Figure 5. It is clearly shown that the twin resonant peaks at $E_c = 2.85$ and 3.24 K are related to $J_e = 6-$ and $4-$, respectively, and they both reach an average lifetime of ~ 100 ps. The $L = 6$ shape resonance at 7.86 K (labeled by $J_e = 5+$ in Figure 5) has a slightly shorter lifetime of ~ 10 ps. Other total angular momenta are not related to the resonances and they do not show long-lived features.

It is interesting to note that the $m = 0$ component has essentially no contribution near the resonance at $E_c = 2.85$ K. In other words, this resonant peak can be completely shut off by H-SARP. In the meantime, the V-SARP ICS is only half of unoriented case, which suggests that while the $|m = -1\rangle$ and $|m = +1\rangle$ components are resonantly enhanced, their scattering amplitudes are anti-synchronous. In V-SARP, as a result, the quantum interference of two pure substates in the equal-weighted superposition state leads to a destructive effect. Since pure states $|m = \pm 1\rangle$ cannot be prepared by SARP, a direct observation of the interference effect is impossible. However, it is possible to prepare SARP states that can unravel quantum interference. In such a set up referred to as X-SARP, two uniaxial states, and a biaxial state can be prepared by using SARP with a cross-polarized pump and Stokes laser fields.²⁰ The biaxial state can be considered as a superposition state of the uniaxial states. As a result, a comparison of the two allows the extraction of effect of the quantum interference.

Such an X-SARP experiment is possible for the current system. To this end, we consider the $0_{0,0+} \leftarrow 2_{0,2+}$ transition for *para*- H_2O . By setting $\beta = \pm \pi/4$, the wave functions of two uniaxial states ϕ_{\pm} are expressed as,

$$\begin{aligned} |2_{0,2}\rangle_{\pm} &= \sum_m d_{0,m}^2(\beta = \pm \pi/4) |m\rangle \\ &= 0.25|0\rangle \pm 0.612(|+1\rangle - |-1\rangle) + 0.306(|+2\rangle + |-2\rangle) \end{aligned} \quad (10)$$

On the other hand, the biaxial state ϕ_X is defined as

$$|2_{0,2}\rangle_X = \frac{1}{\sqrt{2}}(|+1\rangle - |-1\rangle) \quad (11)$$

Using eqs 10 and (11), it is clear that the biaxial state can be regarded as superposition of the two uniaxial states:

$$|2_{0,2}\rangle_X = 0.577(|2_{0,2}\rangle_+ - |2_{0,2}\rangle_-) \quad (12)$$

which suggests the corresponding DCS is

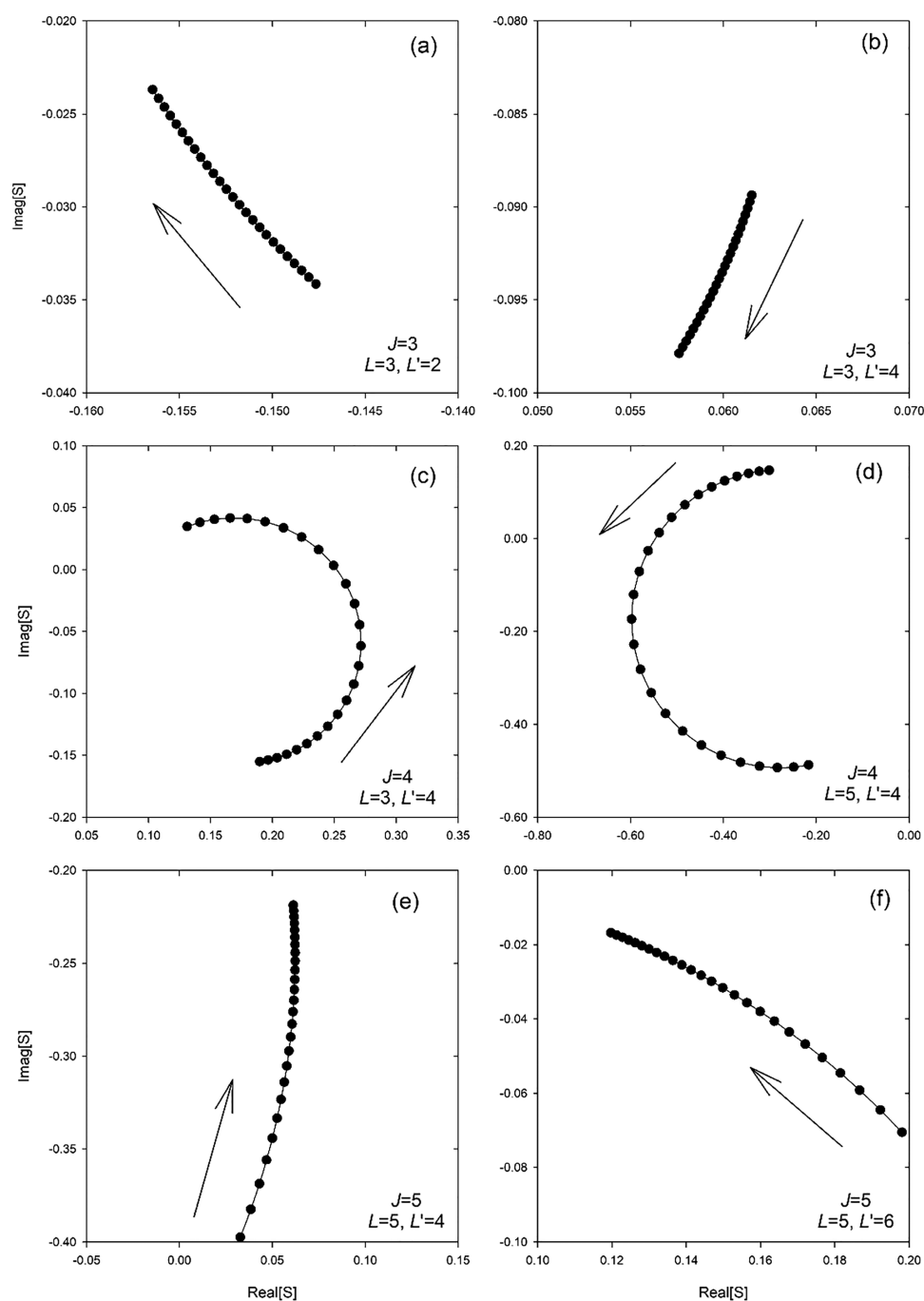


Figure 4. Evolution of S-matrix elements in the complex plane for the $1_{0,1}^- \leftarrow 1_{1,0}^-$ transition for *ortho*-H₂O + He collision. The arrow shows the trajectory as the collision-matrix energy increases from 3.06 to 3.44 K with an interval of 0.014 K.

$$\begin{aligned}
 \left(\frac{d\sigma}{d\Omega}\right)_X &\equiv |q_X|^2 = 0.577^2 |q_+ - q_-|^2 \\
 &= 0.577^2 (|q_+|^2 + |q_-|^2 - q_+^* q_- - q_+ q_-^*) \\
 &= 0.577^2 \left[\left(\frac{d\sigma}{d\Omega}\right)_+ + \left(\frac{d\sigma}{d\Omega}\right)_- - I_{\text{int}} \right], \quad (13)
 \end{aligned}$$

where I_{int} is the interference term between the scattering amplitudes of two uniaxial states.

Figure 6a shows the ICS as a function of collision energy for $|2_{0,2}\rangle_{\pm}$, $|2_{0,2}\rangle_X$ and unoriented cases, where a few resonances are present and their positions are similar to those reported by

Yang and Stancil for scattering of unoriented H₂O by He.³⁶ We will focus on the peaks at $E_c = 3.28$ and 8.06 K, which are related to those discussed above. Similar to the $j = 1$ case, these two shape resonances solely stem from the $L = 5$ and 6 partial waves, respectively, but the former one is much stronger. We present the DCSs at the resonant energy $E_c = 3.28$ K in Figure 6b, in which the red solid line shows the sum of DCSs over two uniaxial states and the black dashed line shows the DCSs of the biaxial state divided by 0.577². This allows one to directly compare scattering intensities with and without the coherence. Both forward and backward scatterings have large differences, indicating quite significant quantum interference effects.

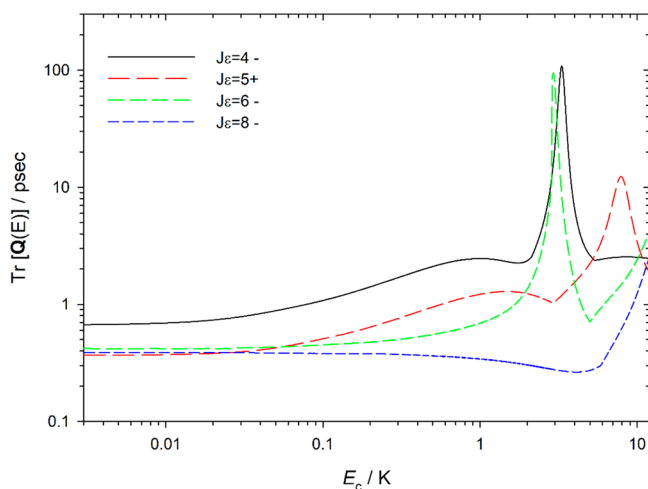


Figure 5. Trace of Smith's lifetime matrix as a function of collision energy for some selected total angular momenta.

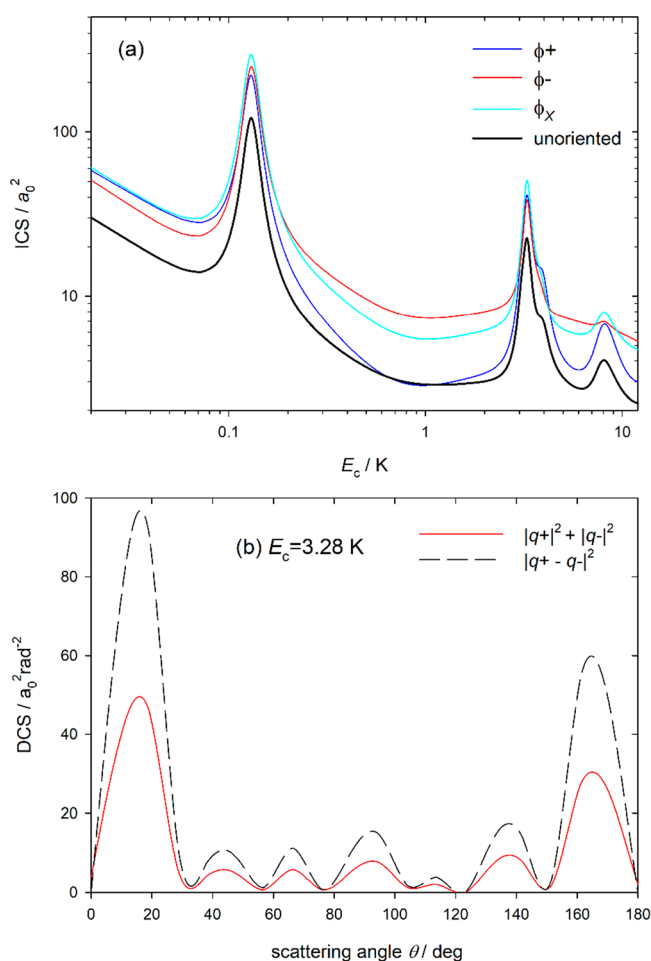


Figure 6. Integral and differential cross sections of the $0_{0,0+} \leftarrow 2_{0,2+}$ transition for *para*-H₂O + He collision. H₂O is prepared in several orientations, where the biaxial state ϕ_x coherently superposes two uniaxial ones ϕ_{\pm} . (a) ICSs for different initially oriented H₂O. (b) Comparison of DCSs with/without coherence at the shape resonant energy.

To summarize, we present the theoretical framework for analyzing stereodynamics in nonreactive atom-molecule scattering in which the molecule is oriented by SARP. The

integral and differential cross sections for the scattering of the oriented molecule can be obtained from numerically exact quantum scattering calculations, which provide the complete description of the scattering dynamics. This analysis is performed for rotational quenching of sterically oriented/unoriented H₂O in collision with He at cold temperatures. It is shown that the stereodynamics is significantly accentuated at low collision energies by shape resonances assignable to one or few partial waves, much the same way as in the SARP experiments involving diatoms. In one case, we demonstrate that it is possible to switch on and off a resonance using SARP. In another example, we show that SARP can be used to extract the effect of quantum interference near a resonance. These new insights help to gain a deeper understanding of the interaction in collision processes.

AUTHOR INFORMATION

Corresponding Authors

Daiqian Xie – Institute of Theoretical and Computational Chemistry, Key Laboratory of Mesoscopic Chemistry, School of Chemistry and Chemical Engineering, Nanjing University, Nanjing 210093, China; orcid.org/0000-0001-7185-7085; Email: dqxie@nju.edu.cn

Hua Guo – Department of Chemistry and Chemical Biology, University of New Mexico, Albuquerque, New Mexico 87131, United States; orcid.org/0000-0001-9901-053X; Email: hguo@unm.edu

Author

Dongzheng Yang – Department of Chemistry and Chemical Biology, University of New Mexico, Albuquerque, New Mexico 87131, United States; orcid.org/0000-0002-8567-1051

Complete contact information is available at: <https://pubs.acs.org/10.1021/acs.jpcllett.2c00187>

Notes

The authors declare no competing financial interest.

ACKNOWLEDGMENTS

This work was supported by a MURI grant from the Army Research Office (Grant No. W911NF-19-1-0283 to H.G.) and in part by the National Natural Science Foundation of China (Grant No. 21733006 to D.X.). The computation was performed at the Center for Advanced Research Computing (CARC) at UNM. We thank Prof. Hui Li for sending us the He–H₂O PES and Prof. Balakrishnan Naduvalath for stimulating discussions.

REFERENCES

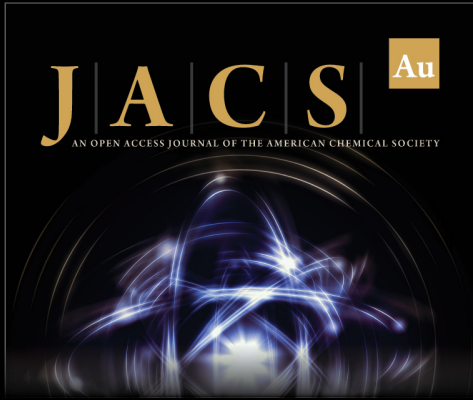
- (1) Krems, R. V. Cold controlled chemistry. *Phys. Chem. Chem. Phys.* **2008**, *10*, 4079–4092.
- (2) Bohn, J. L.; Rey, A. M.; Ye, J. Cold molecules: Progress in quantum engineering of chemistry and quantum matter. *Science* **2017**, *357*, 1002–1010.
- (3) Ni, K.-K.; Ospelkaus, S.; de Miranda, M. H. G.; Pe'er, A.; Neyenhuis, B.; Zirbel, J. J.; Kotochigova, S.; Julienne, P. S.; Jin, D. S.; Ye, J. A high phase-space-density gas of polar molecules. *Science* **2008**, *322*, 231–235.
- (4) Ospelkaus, S.; Ni, K.-K.; Wang, D.; de Miranda, M. H. G.; Neyenhuis, B.; Quémener, G.; Julienne, P. S.; Bohn, J. L.; Jin, D. S.; Ye, J. Quantum-state controlled chemical reactions of ultracold potassium-rubidium molecules. *Science* **2010**, *327*, 853–857.

- (5) Hu, M.-G.; Liu, Y.; Nichols, M. A.; Zhu, L.; Quémener, G.; Dulieu, O.; Ni, K.-K. Nuclear spin conservation enables state-to-state control of ultracold molecular reactions. *Nat. Chem.* **2021**, *13*, 435–440.
- (6) Liu, Y.; Hu, M.-G.; Nichols, M. A.; Yang, D.; Xie, D.; Guo, H.; Ni, K.-K. Precision test of statistical dynamics with state-to-state ultracold chemistry. *Nature* **2021**, *593*, 379–384.
- (7) Gilijamse, J. J.; Hoekstra, S.; van de Meerakker, S. Y. T.; Groenenboom, G. C.; Meijer, G. Near-threshold inelastic collisions using molecular beams with a tunable velocity. *Science* **2006**, *313*, 1617–1620.
- (8) Kirste, M.; Wang, X.; Schewe, H. C.; Meijer, G.; Liu, K.; van der Avoird, A.; Janssen, L. M. C.; Gubbels, K. B.; Groenenboom, G. C.; van de Meerakker, S. Y. T. Quantum-state resolved bimolecular collisions of velocity-controlled OH with NO radicals. *Science* **2012**, *338*, 1060–1063.
- (9) de Jongh, T.; Besemer, M.; Shuai, Q.; Karman, T.; van der Avoird, A.; Groenenboom, G. C.; van de Meerakker, S. Y. T. Imaging the onset of the resonance regime in low-energy NO-He collisions. *Science* **2020**, *368*, 626.
- (10) Perreault, W. E.; Mukherjee, N.; Zare, R. N. Quantum control of molecular collisions at 1 K. *Science* **2017**, *358*, 356–359.
- (11) Perreault, W. E.; Mukherjee, N.; Zare, R. N. Cold quantum-controlled rotationally inelastic scattering of HD with H₂ and D₂ reveals collisional partner reorientation. *Nat. Chem.* **2018**, *10*, 561–567.
- (12) Amarasinghe, C.; Li, H.; Perera, C. A.; Besemer, M.; Zuo, J.; Xie, C.; van der Avoird, A.; Groenenboom, G. C.; Guo, H.; Klos, J.; et al. State-to-state scattering of highly vibrationally excited NO at broadly tunable energies. *Nat. Chem.* **2020**, *12*, 528–534.
- (13) Amarasinghe, C.; Perera, C. A.; Li, H.; Zuo, J.; Besemer, M.; van der Avoird, A.; Groenenboom, G. C.; Guo, H.; Suits, A. G. Collision-induced spin-orbit relaxation of highly vibrationally excited NO near 1 K. *Natural Sci.* **2022**, *2*, No. e20210074.
- (14) Orr-Ewing, A. J.; Zare, R. N. Orientation and alignment of reaction products. *Annu. Rev. Phys. Chem.* **1994**, *45*, 315–366.
- (15) Aoiz, F. J.; Brouard, M.; Gordon, S. D. S.; Nichols, B.; Stolte, S.; Walpole, V. A new perspective: imaging the stereochemistry of molecular collisions. *Phys. Chem. Chem. Phys.* **2015**, *17*, 30210–30228.
- (16) Ni, K. K.; Ospelkaus, S.; Wang, D.; Quémener, G.; Neyenhuis, B.; de Miranda, M. H. G.; Bohn, J. L.; Ye, J.; Jin, D. S. Dipolar collisions of polar molecules in the quantum regime. *Nature* **2010**, *464*, 1324–1328.
- (17) Weck, P. F.; Balakrishnan, N. Importance of long-range interactions in chemical reactions at cold and ultracold temperatures. *Int. Rev. Phys. Chem.* **2006**, *25*, 283–311.
- (18) Naulin, C.; Costes, M. Experimental search for scattering resonances in near cold molecular collisions. *Int. Rev. Phys. Chem.* **2014**, *33*, 427–446.
- (19) Perreault, W. E.; Mukherjee, N.; Zare, R. N. Stark-induced adiabatic Raman passage examined through the preparation of D₂ ($v = 2, j = 0$) and D₂ ($v = 2, j = 2, m = 0$). *J. Chem. Phys.* **2019**, *150*, 234201.
- (20) Zhou, H.; Perreault, W. E.; Mukherjee, N.; Zare, R. N. Quantum mechanical double slit for molecular scattering. *Science* **2021**, *374*, 960–964.
- (21) Zhou, H.; Perreault, W. E.; Mukherjee, N.; Zare, R. N. Shape resonance determined from angular distribution in D₂ ($v = 2, j = 2$) + He → D₂ ($v = 2, j = 0$) + He cold scattering. *J. Chem. Phys.* **2021**, *154*, 104309.
- (22) Zhou, H.; Perreault, W. E.; Mukherjee, N.; Zare, R. N. Highly anisotropic resonant dynamics in the aligned-aligned scattering of cold diatoms. *Nat. Chem.* **2022**, DOI: 10.21203/rs.3.rs-356225/v1.
- (23) Mukherjee, N.; Zare, R. N. Stark-induced adiabatic Raman passage for preparing polarized molecules. *J. Chem. Phys.* **2011**, *135*, No. 024201.
- (24) Perreault, W. E.; Zhou, H.; Mukherjee, N.; Zare, R. N. Harnessing the power of adiabatic curve crossing to populate the highly vibrationally excited H₂ ($v = 7, j = 0$) level. *Phys. Rev. Lett.* **2020**, *124*, 163202.
- (25) Croft, J. F. E.; Balakrishnan, N.; Huang, M.; Guo, H. Unraveling the stereodynamics of cold controlled HD-H₂ collisions. *Phys. Rev. Lett.* **2018**, *121*, 113401.
- (26) Croft, J. F. E.; Balakrishnan, N. Controlling rotational quenching rates in cold molecular collisions. *J. Chem. Phys.* **2019**, *150*, 164302.
- (27) Jambrina, P. G.; Croft, J. F. E.; Guo, H.; Brouard, M.; Balakrishnan, N.; Aoiz, F. J. Stereodynamical control of a quantum scattering resonance in cold molecular collisions. *Phys. Rev. Lett.* **2019**, *123*, No. 043401.
- (28) Morita, M.; Yao, Q.; Xie, C.; Guo, H.; Balakrishnan, N. Stereodynamic control of overlapping resonances with aligned cold molecular collisions. *Phys. Rev. Res.* **2020**, *2*, No. 032018.
- (29) Jambrina, P. G.; Croft, J. F. E.; Balakrishnan, N.; Aoiz, F. J. Stereodynamic control of cold rotationally inelastic CO + HD collisions. *Phys. Chem. Chem. Phys.* **2021**, *23*, 19364–19374.
- (30) Morita, M.; Balakrishnan, N. Stereodynamics of rotationally inelastic scattering in cold He + HD collisions. *J. Chem. Phys.* **2020**, *153*, No. 091101.
- (31) van Dishoeck, E. F.; Herbst, E.; Neufeld, D. A. Interstellar water chemistry: From laboratory to observations. *Chem. Rev.* **2013**, *113*, 9043–9085.
- (32) Bickes, R. W.; Duquette, G.; Meijdenberg, C. J. N. v. d.; Rulis, A. M.; Scoles, G.; Smith, K. M. Molecular beam scattering experiments with polar molecules: measurement of differential collision cross sections for H₂O+H₂, He, Ne, Ar, H₂O and NH₃+H₂, He, NH₃. *J. Phys. B: Atom. Mole. Phys.* **1975**, *8*, 3034–3043.
- (33) Green, S. Collisional excitation of interstellar molecules - Water. *Astrophys. J. Supp. Ser.* **1980**, *42*, 103–141.
- (34) Bruderer, J.; Steinbach, C.; Buck, U.; Patkowski, K.; Moszynski, R. Elastic and rotationally inelastic differential cross sections for He+H₂O collisions. *J. Chem. Phys.* **2002**, *117*, 11166–11174.
- (35) Cappelletti, D.; Aquilanti, V.; Cornicchi, E.; Teixidor, M. M.; Pirani, F. Molecular-beam study of the water-helium system: Features of the isotropic component of the intermolecular interaction and a critical test for the available potential-energy surfaces. *J. Chem. Phys.* **2005**, *123*, No. 024302.
- (36) Yang, B.; Stancil, P. C. Close-coupling study of rotational energy transfer and differential scattering in H₂O collisions with He atoms. *J. Chem. Phys.* **2007**, *126*, 154306.
- (37) Yang, C.-H.; Sarma, G.; ter Meulen, J. J.; Parker, D. H.; Buck, U.; Wiesenfeld, L. Imaging the inelastic scattering of water with helium. Comparison of experiment and theory. *J. Phys. Chem. A* **2010**, *114*, 9886–9892.
- (38) Sarma, G.; Saha, A. K.; Bishwakarma, C. K.; Scheidsbach, R.; Yang, C.-H.; Parker, D.; Wiesenfeld, L.; Buck, U.; Mavridis, L.; Marinakis, S. Collision energy dependence of state-to-state differential cross sections for rotationally inelastic scattering of H₂O by He. *Phys. Chem. Chem. Phys.* **2017**, *19*, 4678–4687.
- (39) Yang, D.; Xie, D.; Guo, H. A time-independent quantum approach to ro-vibrationally inelastic scattering between atoms and triatomic molecules. *J. Phys. Chem. A* **2021**, *125*, 6864–6871.
- (40) Hou, D.; Ma, Y.-T.; Zhang, X.-L.; Li, H. A full-dimension intra- and inter-molecular ab initio potential energy surface and predicted infrared spectra for H₂O-He. *J. Mol. Spectrosc.* **2016**, *330*, 217–227.
- (41) Arthurs, A. M.; Dalgarno, A. The theory of scattering by a rigid rotator. *Proc. Royal Soc. A* **1960**, *256*, 540–551.
- (42) Garrison, B. J.; Lester, W. A.; Miller, W. H. Coupled-channel study of rotational excitation of a rigid asymmetric top by atom impact: (H₂CO,He) at interstellar temperatures. *J. Chem. Phys.* **1976**, *65*, 2193–2200.
- (43) Alexander, M. H.; Dagdigan, P. J.; DePristo, A. E. Quantum interpretation of fully state-selected rotationally inelastic collision experiments. *J. Chem. Phys.* **1977**, *66*, 59–66.


(44) Alexander, M. H. Close-coupling studies of the orientation dependence of rotationally inelastic collisions. *J. Chem. Phys.* **1977**, *67*, 2703–2712.

(45) Smith, F. T. Lifetime matrix in collision theory. *Phys. Rev.* **1960**, *118*, 349–356.


(46) González-Martínez, M. L.; Hutson, J. M. Ultracold atom-molecule collisions and bound states in magnetic fields: Tuning zero-energy Feshbach resonances in He-NH($^3\Sigma^-$). *Phys. Rev. A* **2007**, *75*, No. 022702.




JACS Au
AN OPEN ACCESS JOURNAL OF THE AMERICAN CHEMICAL SOCIETY



Editor-in-Chief
Prof. Christopher W. Jones
Georgia Institute of Technology, USA

Open for Submissions 

pubs.acs.org/jacsau  ACS Publications
Most Trusted. Most Cited. Most Read.